Search for Chargino and Neutralino Production in e^+e^- Collisions at $\sqrt{s} = 161$ GeV

The OPAL Collaboration

Abstract

Charginos and neutralinos, predicted by supersymmetric theories, have been searched for in e^+e^- collisions with an integrated luminosity of 10.0 pb^{-1} at a centre-of-mass energy of $\sqrt{s}$ =161 GeV with the OPAL detector at LEP. Two candidate events are selected; consistent with the total background estimate of 0.7 ± 0.2 events. The 95% C.L. lower limit on the lightest chargino mass in the Minimal Supersymmetric Standard Model is 78.5 GeV if the universal scalar mass m_0 is greater than 1 TeV, and 62.0 GeV for the smallest m_0 compatible with slepton and sneutrino mass limits obtained at centre-of-mass energies near the Z peak. These limits were obtained under the conditions that the lightest chargino is heavier than the lightest neutralino by more than 10 GeV and $\tan\beta = 1.5$. The new exclusion limits significantly improve on the results obtained at $\sqrt{s}$ =130 and 136 GeV.

Submitted to Physics Letters B

The OPAL Collaboration

K. Ackerstaff[8], G. Alexander[23], J. Allison[16], N. Altekamp[5], K. Ametewee[25], K.J. Anderson[9],
S. Anderson[12], S. Arcelli[2], S. Asai[24], D. Axen[29], G. Azuelos[18,a], A.H. Ball[17], E. Barberio[8],
R.J. Barlow[16], R. Bartoldus[3], J.R. Batley[5], J. Bechtluft[14], C. Beeston[16], T. Behnke[8], A.N. Bell[1],
K.W. Bell[20], G. Bella[23], S. Bentvelsen[8], P. Berlich[10], S. Bethke[14], O. Biebel[14], V. Blobel[27],
I.J. Bloodworth[1], J.E. Bloomer[1], M. Bobinski[10], P. Bock[11], H.M. Bosch[11], M. Boutemeur[34],
B.T. Bouwens[12], S. Braibant[12], R.M. Brown[20], H.J. Burckhart[8], C. Burgard[8], R. Bürgin[10],
P. Capiluppi[2], R.K. Carnegie[6], A.A. Carter[13], J.R. Carter[5], C.Y. Chang[17], D.G. Charlton[1,b],
D. Chrisman[4], P.E.L. Clarke[15], I. Cohen[23], J.E. Conboy[15], O.C. Cooke[16], M. Cuffiani[2],
S. Dado[22], C. Dallapiccola[17], G.M. Dallavalle[2], S. De Jong[12], L.A. del Pozo[8], K. Desch[3],
M.S. Dixit[7], E. do Couto e Silva[12], M. Doucet[18], E. Duchovni[26], G. Duckeck[34], I.P. Duerdoth[16],
J.E.G. Edwards[16], P.G. Estabrooks[6], H.G. Evans[9], M. Evans[13], F. Fabbri[2], P. Fath[11],
F. Fiedler[27], M. Fierro[2], H.M. Fischer[3], R. Folman[26], D.G. Fong[17], M. Foucher[17], A. Fürtjes[8],
P. Gagnon[7], J.W. Gary[4], J. Gascon[18], S.M. Gascon-Shotkin[17], N.I. Geddes[20], C. Geich-Gimbel[3],
T. Geralis[20], G. Giacomelli[2], P. Giacomelli[4], R. Giacomelli[2], V. Gibson[5], W.R. Gibson[13],
D.M. Gingrich[30,a], D. Glenzinski[9], J. Goldberg[22], M.J. Goodrick[5], W. Gorn[4], C. Grandi[2],
E. Gross[26], J. Grunhaus[23] M. Gruwé[8], C. Hajdu[32], G.G. Hanson[12], M. Hansroul[8], M. Hapke[13],
C.K. Hargrove[7], P.A. Hart[9], C. Hartmann[3], M. Hauschild[8], C.M. Hawkes[5], R. Hawkings[8],
R.J. Hemingway[6], M. Herndon[17], G. Herten[10], R.D. Heuer[8], M.D. Hildreth[8], J.C. Hill[5],
S.J. Hillier[1], T. Hilse[10], P.R. Hobson[25], R.J. Homer[1], A.K. Honma[28,a], D. Horváth[32,c],
R. Howard[29], R.E. Hughes-Jones[16], D.E. Hutchcroft[5], P. Igo-Kemenes[11], D.C. Imrie[25],
M.R. Ingram[16], K. Ishii[24], A. Jawahery[17], P.W. Jeffreys[20], H. Jeremie[18], M. Jimack[1], A. Joly[18],
C.R. Jones[5], G. Jones[16], M. Jones[6], R.W.L. Jones[8], U. Jost[11], P. Jovanovic[1], T.R. Junk[8],
D. Karlen[6], K. Kawagoe[24], T. Kawamoto[24], R.K. Keeler[28], R.G. Kellogg[17], B.W. Kennedy[20],
B.J. King[8], J. Kirk[29], S. Kluth[8], T. Kobayashi[24], M. Kobel[10], D.S. Koetke[6], T.P. Kokott[3],
M. Kolrep[10], S. Komamiya[24], T. Kress[11], P. Krieger[6], J. von Krogh[11], P. Kyberd[13],
G.D. Lafferty[16], R. Lahmann[17], W.P. Lai[19], D. Lanske[14], J. Lauber[15], S.R. Lautenschlager[31],
J.G. Layter[4], D. Lazic[22], A.M. Lee[31], E. Lefebvre[18], D. Lellouch[26], J. Letts[2], L. Levinson[26],
C. Lewis[15], S.L. Lloyd[13], F.K. Loebinger[16], G.D. Long[17], M.J. Losty[7], J. Ludwig[10],
M. Mannelli[8], S. Marcellini[2], C. Markus[3], A.J. Martin[13], J.P. Martin[18], G. Martinez[17],
T. Mashimo[24], W. Matthews[25], P. Mättig[3], W.J. McDonald[30], J. McKenna[29], E.A. Mckigney[15],
T.J. McMahon[1], A.I. McNab[13], R.A. McPherson[8], F. Meijers[8], S. Menke[3], F.S. Merritt[9],
H. Mes[7], J. Meyer[27], A. Michelini[2], G. Mikenberg[26], D.J. Miller[15], R. Mir[26], W. Mohr[10],
A. Montanari[2], T. Mori[24], M. Morii[24], U. Müller[3], K. Nagai[26], I. Nakamura[24], H.A. Neal[8],
B. Nellen[3], B. Nijjhar[16], R. Nisius[8], S.W. O'Neale[1], F.G. Oakham[7], F. Odorici[2], H.O. Ogren[12],
N.J. Oldershaw[16], T. Omori[24], M.J. Oreglia[9], S. Orito[24], J. Pálinkás[33,d], G. Pásztor[32],
J.R. Pater[16], G.N. Patrick[20], J. Patt[10], M.J. Pearce[1], S. Petzold[27], P. Pfeifenschneider[14],
J.E. Pilcher[9], J. Pinfold[30], D.E. Plane[8], P. Poffenberger[28], B. Poli[2], A. Posthaus[3],
H. Przysiezniak[30], D.L. Rees[1], D. Rigby[1], S. Robertson[28], S.A. Robins[13], N. Rodning[30],
J.M. Roney[28], A. Rooke[15], E. Ros[8], A.M. Rossi[2], M. Rosvick[28], P. Routenburg[30], Y. Rozen[22],
K. Runge[10], O. Runolfsson[8], U. Ruppel[14], D.R. Rust[12], R. Rylko[25], K. Sachs[10],
E.K.G. Sarkisyan[23], M. Sasaki[24], C. Sbarra[2], A.D. Schaile[34], O. Schaile[34], F. Scharf[3],
P. Scharff-Hansen[8], P. Schenk[27], B. Schmitt[8], S. Schmitt[11], M. Schröder[8],
H.C. Schultz-Coulon[10], M. Schulz[8], M. Schumacher[3], P. Schütz[3], W.G. Scott[20], T.G. Shears[16],
B.C. Shen[4], C.H. Shepherd-Themistocleous[8], P. Sherwood[15], G.P. Siroli[2], A. Sittler[27],

A. Skillman[15], A. Skuja[17], A.M. Smith[8], T.J. Smith[28], G.A. Snow[17], R. Sobie[28],
S. Söldner-Rembold[10], R.W. Springer[30], M. Sproston[20], A. Stahl[3], M. Steiert[11], K. Stephens[16],
J. Steuerer[27], B. Stockhausen[3], D. Strom[19], F. Strumia[8], P. Szymanski[20], R. Tafirout[18],
S.D. Talbot[1], S. Tanaka[24], P. Taras[18], S. Tarem[22], M. Thiergen[10], M.A. Thomson[8], E. von
Törne[3], S. Towers[6], I. Trigger[18], T. Tsukamoto[24], E. Tsur[23], A.S. Turcot[9],
M.F. Turner-Watson[8], P. Utzat[11], R. Van Kooten[12], M. Verzocchi[10], P. Vikas[18], M. Vincter[28],
E.H. Vokurka[16], F. Wäckerle[10], A. Wagner[27], C.P. Ward[5], D.R. Ward[5], J.J. Ward[15],
P.M. Watkins[1], A.T. Watson[1], N.K. Watson[7], P.S. Wells[8], N. Wermes[3], J.S. White[28],
B. Wilkens[10], G.W. Wilson[27], J.A. Wilson[1], G. Wolf[26], S. Wotton[5], T.R. Wyatt[16],
S.. Yamashita[24], G. Yekutieli[26], V. Zacek[18],

[1]School of Physics and Space Research, University of Birmingham, Birmingham B15 2TT, UK
[2]Dipartimento di Fisica dell' Università di Bologna and INFN, I-40126 Bologna, Italy
[3]Physikalisches Institut, Universität Bonn, D-53115 Bonn, Germany
[4]Department of Physics, University of California, Riverside CA 92521, USA
[5]Cavendish Laboratory, Cambridge CB3 0HE, UK
[6] Ottawa-Carleton Institute for Physics, Department of Physics, Carleton University, Ottawa,
Ontario K1S 5B6, Canada
[7]Centre for Research in Particle Physics, Carleton University, Ottawa, Ontario K1S 5B6,
Canada
[8]CERN, European Organisation for Particle Physics, CH-1211 Geneva 23, Switzerland
[9]Enrico Fermi Institute and Department of Physics, University of Chicago, Chicago IL 60637,
USA
[10]Fakultät für Physik, Albert Ludwigs Universität, D-79104 Freiburg, Germany
[11]Physikalisches Institut, Universität Heidelberg, D-69120 Heidelberg, Germany
[12]Indiana University, Department of Physics, Swain Hall West 117, Bloomington IN 47405,
USA
[13]Queen Mary and Westfield College, University of London, London E1 4NS, UK
[14]Technische Hochschule Aachen, III Physikalisches Institut, Sommerfeldstrasse 26-28, D-52056
Aachen, Germany
[15]University College London, London WC1E 6BT, UK
[16]Department of Physics, Schuster Laboratory, The University, Manchester M13 9PL, UK
[17]Department of Physics, University of Maryland, College Park, MD 20742, USA
[18]Laboratoire de Physique Nucléaire, Université de Montréal, Montréal, Quebec H3C 3J7,
Canada
[19]University of Oregon, Department of Physics, Eugene OR 97403, USA
[20]Rutherford Appleton Laboratory, Chilton, Didcot, Oxfordshire OX11 0QX, UK
[22]Department of Physics, Technion-Israel Institute of Technology, Haifa 32000, Israel
[23]Department of Physics and Astronomy, Tel Aviv University, Tel Aviv 69978, Israel
[24]International Centre for Elementary Particle Physics and Department of Physics, University
of Tokyo, Tokyo 113, and Kobe University, Kobe 657, Japan
[25]Brunel University, Uxbridge, Middlesex UB8 3PH, UK
[26]Particle Physics Department, Weizmann Institute of Science, Rehovot 76100, Israel
[27]Universität Hamburg/DESY, II Institut für Experimental Physik, Notkestrasse 85, D-22607
Hamburg, Germany
[28]University of Victoria, Department of Physics, P O Box 3055, Victoria BC V8W 3P6, Canada

^{29}University of British Columbia, Department of Physics, Vancouver BC V6T 1Z1, Canada
^{30}University of Alberta, Department of Physics, Edmonton AB T6G 2J1, Canada
^{31}Duke University, Dept of Physics, Durham, NC 27708-0305, USA
^{32}Research Institute for Particle and Nuclear Physics, H-1525 Budapest, P O Box 49, Hungary
^{33}Institute of Nuclear Research, H-4001 Debrecen, P O Box 51, Hungary
^{34}Ludwigs-Maximilians-Universität München, Sektion Physik, Am Coulombwall 1, D-85748 Garching, Germany

[a] and at TRIUMF, Vancouver, Canada V6T 2A3
[b] and Royal Society University Research Fellow
[c] and Institute of Nuclear Research, Debrecen, Hungary
[d] and Department of Experimental Physics, Lajos Kossuth University, Debrecen, Hungary

1 Introduction

In summer 1996 the LEP e^+e^- collider at CERN was run for the first time at a centre-of-mass energy ($\sqrt{s}$) of 161 GeV. This provided an opportunity to search for new particles in this new energy region. In this publication we report on a direct search for charginos and neutralinos predicted in supersymmetric (SUSY) theories [1] using the data collected with the OPAL detector at $\sqrt{s}$ =161 GeV. We obtain improved exclusion limits compared to the previous results from the analysis of data near the Z peak (LEP1) and at $\sqrt{s} = 130 - 136$ GeV (LEP1.5) at LEP by the OPAL [2] and other LEP collaborations [3]. Similar but more model-dependent limits were also obtained by the CDF and D0 collaborations at the Tevatron [4].

Charginos $\tilde{\chi}_j^\pm$ are the mass eigenstates formed by the mixing of the fields of the fermionic partners of the charged gauge bosons (winos) and those of the charged Higgs bosons (charged higgsinos). Fermionic partners of the γ, the Z boson, and the neutral Higgs bosons mix to form the mass eigenstates called neutralinos $\tilde{\chi}_i^0$. In each case, the index j or i is ordered by increasing mass. Throughout this paper, the lightest neutralino, $\tilde{\chi}_1^0$, is assumed to be the lightest supersymmetric particle and is therefore stable and invisible if R-parity is conserved. We used the Minimal Supersymmetric Standard Model (MSSM) [5] to guide the analysis but more general cases are also studied.

If charginos are light enough, they can be pair-produced in e^+e^- collisions through γ or Z exchange in the s-channel and through sneutrino ($\tilde{\nu}$) exchange in the t-channel. The production cross-section is large unless the sneutrino is light, in which case the cross-section is reduced since destructive interference may occur between the s-channel Z or γ and t-channel $\tilde{\nu}$ exchange diagrams [6, 7].

The details of chargino decay depend on the parameters of the mixing and the masses of the scalar partners of the ordinary fermions. The lightest chargino $\tilde{\chi}_1^\pm$ can decay via $\tilde{\chi}_1^+ \to \tilde{\chi}_1^0 \ell^+ \nu$, or via $\tilde{\chi}_1^+ \to \tilde{\chi}_1^0 q\bar{q}'$, through virtual W, slepton ($\tilde{\ell}$), or scalar quark ($\tilde{q}$) emission. In most of the MSSM parameter space $\tilde{\chi}_1^+$ decay via virtual W emission is dominant. The MSSM predicted cross-sections for $\tilde{\chi}_1^+\tilde{\chi}_1^-$ events are typically several pb.

Due to the energy and momentum carried away by the invisible $\tilde{\chi}_1^0$ and/or neutrinos, the experimental signature for $\tilde{\chi}_1^+\tilde{\chi}_1^-$ events is large missing momentum and acoplanar pairs of particles and/or jets.

Neutralino pairs ($\tilde{\chi}_i^0\tilde{\chi}_j^0$) can be produced through an s-channel virtual Z or γ, or by t-channel selectron ($\tilde{e}$) exchange. The second lightest neutralino, $\tilde{\chi}_2^0$, produced in conjunction with a $\tilde{\chi}_1^0$ may give the first direct signal for neutralinos at LEP[1]. The $\tilde{\chi}_2^0$ would decay into the final states $\tilde{\chi}_1^0\nu\bar{\nu}$, $\tilde{\chi}_1^0\ell^+\ell^-$ or $\tilde{\chi}_1^0 q\bar{q}$ via a Z^*, a neutral SUSY Higgs boson (h^0 or A^0), a scalar neutrino, a scalar lepton, or a scalar quark. This leads to an experimental signature consisting either of an acoplanar pair of particles or jets, or a monojet where the two jets in the final state have merged. In some regions of SUSY parameter space the decay process $\tilde{\chi}_2^0 \to \tilde{\chi}_1^0\gamma$ is possible. However, this final state is not considered in the present publication. The MSSM predicted cross-sections for $\tilde{\chi}_2^0\tilde{\chi}_1^0$ events is typically a fraction of a pb but can vary significantly depending on the choice of MSSM parameters. The $\tilde{\chi}_3^0$ is generally assumed to decay into $\tilde{\chi}_{1,2}^0 Z^*$. We also consider $\tilde{\chi}_3^0$ decays into $\tilde{\chi}_{1,2}^0 h^0$ and $\tilde{\chi}_{1,2}^0 A^0$ and decays where $\tilde{\chi}_3^0 \to \tilde{\chi}_2^0\gamma$ with $\tilde{\chi}_2^0 \to \tilde{\chi}_1^0 Z^*$. These $\tilde{\chi}_3^0$ decays would result in $\tilde{\chi}_1^0\tilde{\chi}_3^0$ events with experimental signatures similar to $\tilde{\chi}_1^0\tilde{\chi}_2^0$.

---

[1]Possible initial state radiative events, $e^+e^- \to \tilde{\chi}_1^0\tilde{\chi}_1^0\gamma$, suffer from backgrounds due to $e^+e^- \to \nu\bar{\nu}\gamma$.

2 The OPAL Detector and Event Simulation

The OPAL detector is described in detail in [8]; it is a multipurpose apparatus having nearly complete solid angle coverage. The central detector consists of a silicon microvertex detector and a system of tracking chambers inside a 0.435 T magnetic field. A lead-glass electromagnetic (EM) calorimeter together with presamplers and time-of-flight scintillators is located outside the magnet coil and at the front of both endcaps. The magnet return yoke is instrumented for hadron calorimetry (HCAL) and is surrounded by external muon chambers. The forward detectors (FD) and silicon tungsten calorimeters (SW) located on both sides of the interaction point measure the luminosity and complete the geometrical acceptance down to 24 mrad in polar angle[2].

The Monte Carlo generator SUSYGEN [9] was used to simulate chargino and neutralino pair events. We also used a Monte Carlo generator based on the calculation of the differential cross-sections by Bartl *et al.* [6] for chargino pair production. In both generators initial state radiation was included and the JETSET 7.4 package [10] was used for the hadronisation of the quark-antiquark system in the chargino or neutralino hadronic decays.

The most important parameters determining the chargino detection efficiency are the mass of the chargino, $m_{\tilde{\chi}_1^+}$, and the mass difference between the chargino and the lightest neutralino, $\Delta M_+ \equiv m_{\tilde{\chi}_1^+} - m_{\tilde{\chi}_1^0}$. For the neutralino detection efficiency, $m_{\tilde{\chi}_2^0}$ and $\Delta M_0 \equiv m_{\tilde{\chi}_2^0} - m_{\tilde{\chi}_1^0}$ are the main parameters that determine the efficiency. We generated $\tilde{\chi}_1^+ \tilde{\chi}_1^-$ events at 48 points in the $(m_{\tilde{\chi}_1^+}, \Delta M_+)$ plane, for $m_{\tilde{\chi}_1^+}$ between 50 GeV and 80 GeV and ΔM_+ between 3 GeV and $m_{\tilde{\chi}_1^+}$. At each point 1000 events for the decay $\tilde{\chi}_1^+ \rightarrow \tilde{\chi}_1^0 W^{*+}$ were generated. For the $\tilde{\chi}_2^0 \tilde{\chi}_1^0$ process, events were generated at 62 points in the $(m_{\tilde{\chi}_1^0}, m_{\tilde{\chi}_2^0})$ plane, for $(m_{\tilde{\chi}_1^0} + m_{\tilde{\chi}_2^0})$ between 90 GeV and 160 GeV and $m_{\tilde{\chi}_1^0}$ between 10 GeV and $(m_{\tilde{\chi}_2^0} - 2.5 \text{ GeV})$. At each point, 2000 events for the decay $\tilde{\chi}_2^0 \rightarrow \tilde{\chi}_1^0 Z^*$ with $Z^* \rightarrow \ell^+ \ell^-$ or $q\bar{q}$ were generated.

The sources of background to the chargino and neutralino signals include two-photon, lepton pair, multihadronic and four-fermion processes. Two-photon processes are the most important background for the case of small ΔM_+, since signal events have small visible energy and small transverse momentum relative to the beam direction. We used the Monte Carlo generators PYTHIA [10], PHOJET [11] and HERWIG [12] for simulating hadronic events from two-photon processes. Four lepton events ($e^+e^- e^+e^-$, $e^+e^- \mu^+\mu^-$ and $e^+e^- \tau^+\tau^-$) were produced by using the Vermaseren program [13]. Four-fermion processes in which at least one of the fermions is a neutrino constitute a serious background. The dominant contributions are W^+W^- or $Z\gamma^*$ events that have topologies very similar to that of the signal. The EXCALIBUR [14] generator, which takes into account all interfering four-fermion diagrams was used to simulate these backgrounds. Events generated using EXCALIBUR do not include $e^+e^- \rightarrow We\nu$ and $e^+e^- \rightarrow (Z^*/\gamma^*)e^+e^-$ events in which one of the electrons scatters at a very small angle. These events were generated using PYTHIA. Lepton pairs were generated using the KORALZ [15] generator for $\tau^+\tau^-(\gamma)$ and $\mu^+\mu^-(\gamma)$ events and the BHWIDE program [16] for $e^+e^- \rightarrow e^+e^-(\gamma)$ events. Multihadronic, $q\bar{q}(\gamma)$, events were simulated using PYTHIA.

Generated signal and background events were processed through the full simulation of the OPAL detector [17] and the same event analysis chain was applied to the simulated events as

---

[2] A right-handed coordinate system is adopted, where the x-axis points to the centre of the LEP ring, and positive z is along the electron beam direction. The angles θ and ϕ are the polar and azimuthal angles, respectively.

to the data.

3   Analysis

The analysis was performed on data collected during the 1996 summer run of LEP at a centre-of-mass energy of $\sqrt{s}$ =161 GeV. Data were used from runs in which all the subdetectors relevant to this analysis were fully operational, corresponding to an integrated luminosity of 10.0 pb^{-1}.

To select good charged tracks and clusters in the calorimeters, quality requirements similar to those in Ref. [2] were applied[3]. Calculations of experimental variables were performed using the four-momenta of tracks and of EM or HCAL clusters not associated with charged tracks[4]. Calorimeter clusters associated with charged tracks were also included after the expected calorimeter energy for the associated charged track momenta was subtracted from the cluster energy to reduce double counting. If the energy of a cluster was smaller than the expected energy for the associated tracks, the cluster energy was not used.

Jets were formed using the Durham algorithm [18] with a jet resolution parameter of y_{cut} = 0.005, unless otherwise specified.

The event sample was divided into three categories, motivated by the topologies expected to result from chargino and neutralino events, and the analysis was optimised for each of them:

(A) $N_{\text{ch}} > 4$ and no isolated lepton, where N_{ch} is the number of charged tracks,

(B) $N_{\text{ch}} > 4$ and at least one isolated lepton, and

(C) $N_{\text{ch}} \leq 4$.

Isolated leptons were identified in the following way. Electrons were selected if they satisfied either of the two identification methods described in [19, 20] and muons were identified using three methods [21, 22, 23]. The momentum of the electron or muon candidate was required to be larger than 2 GeV. A reconstructed jet was identified as a tau decay if there were only one or three charged tracks in the jet, the momentum sum of the charged tracks was larger than 1.5 GeV, the invariant mass of the charged particles in the jet was smaller than 1.5 GeV and the invariant mass of the jet was smaller than the mass of the tau. The lepton was defined to be isolated if the energy within a cone of half angle 25° around the electron, muon or tau candidate was less than 2 GeV.

As a preselection, events were required to have two or more tracks, a total transverse momentum with respect to the beam direction (P_t) exceeding 1 GeV and no energy in each side of the forward detectors above a given threshold (5 GeV for SW and 2 GeV for FD).

---

[3]In the polar angle region of $0.725 < |\cos\theta| < 0.765$ with azimuthal ranges of $0° < \phi < 4.5°$, $265.5° < \phi < 274.5°$ or $175.5° < \phi < 180°$, a significant amount of material is localised in front of the barrel EM calorimeter. If a high-energy photon hits this region, a large amount of its energy is lost and the missing momentum of the event can become large. Events were rejected if a cluster with observed raw energy above 1 GeV was found in this region. The total solid angle of the areas defined above is about 0.2% of 4π.

[4]The masses of all charged particles were set to the charged pion mass and the invariant masses of the calorimeter energy clusters were assumed to be zero.

6

3.1 Category A: Hadronic decays without isolated leptons

If both $\tilde{\chi}_1^+$ and $\tilde{\chi}_1^-$ decay hadronically in $\tilde{\chi}_1^+\tilde{\chi}_1^-$ events or the $\tilde{\chi}_{2,3}^0$ decays hadronically in $\tilde{\chi}_1^0\tilde{\chi}_{2,3}^0$ events then the events tend to fall into category (A). The fraction of $\tilde{\chi}_1^+\tilde{\chi}_1^-$ events falling into category (A) is about 45% for most of the $(m_{\tilde{\chi}_1^\pm}, m_{\tilde{\chi}_1^0})$ region. The fraction drops to about 15% if the difference between $m_{\tilde{\chi}_1^\pm}$ and $m_{\tilde{\chi}_1^0}$ is 5 GeV or less, since the average charged track multiplicity of the events is smaller. For $\tilde{\chi}_1^0\tilde{\chi}_{2,3}^0$ events the fraction is essentially determined by the decay of the virtual Z boson. For mass differences exceeding 80 GeV between $\tilde{\chi}_{2,3}^0$ and $\tilde{\chi}_1^0$ the fraction is typically 80%. This drops to about 40% for a mass difference of 60 GeV, and for a mass difference between $\tilde{\chi}_{2,3}^0$ and $\tilde{\chi}_1^0$ of 5 GeV or less the fraction is approximately 7%.

The major backgrounds in category (A) are from four-fermion (including W^+W^- and Weν), two-photon and $q\bar{q}(\gamma)$ events. The distribution of the visible mass of the events, M_{vis}, is shown in Fig. 1(a) for the events satisfying the preselection requirements. In this distribution, the low mass region is dominated by two-photon processes, while the two high mass peaks are due to annihilation decays and radiative returns to the Z. The various simulated background processes provide a good description of the data. The counts of preselected events for the backgrounds and a typical chargino and neutralino signal are shown in Table 1.

To select well measured and well contained events, more than 85% of the total visible energy was required to be in the central regoin ($|\cos\theta| < 0.9$) and we required that not be any tracks (clusters) with momentum (energy) larger than the beam energy.

Two-photon background events were rejected by cuts on the event transverse momentum, P_t, and on the acoplanarity angle. The $q\bar{q}(\gamma)$ and $\ell^+\ell^-(\gamma)$ background events were also reduced by these cuts as well as a requirement on the longitudinal momentum(P_z) of the events to eliminate radiative Z decays in which the γ is emitted along the beam direction ($|P_z| < 25$ GeV). The majority of the two-photon processes were eliminated by demanding that the P_t exceeds 5 GeV. The remaining two-photon events as well as fully contained multihadronic final states were rejected by demanding that the acoplanarity angle[5] ϕ_{acop} exceeds 20°. The counts of events remaining after the category (A) two-photon and $q\bar{q}(\gamma)$ cuts are shown in the third row of Table 1.

The four-fermion background from W^+W^- and Weν events was reduced using cuts on the reconstructed mass and jet energies. Some of the $W^+W^- \rightarrow q\bar{q}\ell\nu$ events were classified in category (A) due to the reconstructed lepton not passing the isolation requirements of category (B). The lepton in these events was identified using an algorithm optimised to have high efficiency for highly energetic leptons near the jet. The algorithm identified the lepton by requiring that there be significant momentum (> 5 GeV), visible mass less than 2.5 GeV and less than 7.5 GeV deposited in either the EM calorimeter or HCAL (for $\mu^\pm$ and $\tau^\pm$ candidates) within a cone of half angle 5°(7.5°) if the cone contained 1(3) track(s). Then, loose isolation requirements based on the fraction of energy and number of tracks between this cone and a cone of half angle 25° about the same direction were applied to ensure correctness of the lepton identification cuts. Events containing such a lepton where the mass of the system recoiling against it was consistent with the W mass (55 to 110 GeV) were rejected. The fact that W and Z decays give rise to energetic jets was used to reject events with either multihadronic final

---

[5]For category (A), ϕ_{acop} is defined as 180°$-$ the angle, projected into the plane perpendicular to the beam direction, between the directions of the two momentum vectors of the hemispheres obtained by dividing the event by a plane perpendicular to the thrust axis. If there are no reconstructed clusters or tracks in one of the hemispheres, the event is considered to be a monojet and ϕ_{acop} is set to 180°.

states, where some of the particles escaped detection along the beam direction, or W$e\nu$ final states, where the electron travelled close to the beam direction. The second most energetic jet in the event was required to have an energy of less than 25 GeV for events containing three or more jets, and less than 30 GeV for events containing two jets. This requirement was needed to retain high efficiency in the case of neutralino pair production, where two high energy jets were produced. Most of the remaining W$e\nu$ events were eliminated by requiring that the observed visible mass of the event does not lie between 60 and 80 GeV for events with three or fewer jets. Remaining events from W decays were due to final states containing multiple jets that were not eliminated by the cut on the energy of the second most energetic jet. Their contribution is reduced by demanding that the most energetic jet in the event has an energy smaller than 30 GeV, if the transition from two to three jet topology occurred at a y_{cut} value greater than 0.02. The counts of events remaining after the category (A) four-fermion cuts are shown in the fourth row of Table 1.

One event survived the above cuts and is shown in Fig. 2. The event has a charged multiplicity of 16, 4 jets, a visible energy of 55 GeV and missing transverse momentum of 39 GeV. The recoil mass of the event, 99 GeV, is within 1 σ of the Z boson mass. This event may be due to ZZ$^{*} \rightarrow \nu\bar{\nu}q\bar{\mathrm{q}}$ or Z$\gamma^{*} \rightarrow \nu\bar{\nu}q\bar{\mathrm{q}}$. The acoplanarity angle distribution after all the other cuts are applied is shown in Fig. 1(b) for data including the surviving event and simulated background events. A typical chargino signal is also plotted in the figure. For events falling into category (A) the detection efficiency for $\tilde{\chi}_1^+\tilde{\chi}_1^-$ events is typically 40–60% for ΔM_+ between 10 GeV and $m_{\tilde{\chi}_1^+}/2$ and for $\tilde{\chi}_2^0\tilde{\chi}_1^0$ events it is typically 20–45% for ΔM_0 between 20 GeV and 70 GeV. The total number of background events expected in category (A) is 0.36.

cut	data	net bkg.	q$\bar{\mathrm{q}}(\gamma)$	$\ell^+\ell^-(\gamma)$	'$\gamma\gamma$'	4-f	$\tilde{\chi}_1^+\tilde{\chi}_1^-$ (%)	$\tilde{\chi}_2^0\tilde{\chi}_1^0$ (%)
Category (A)	–	–	–	–	–	–	33.3	74.5
Preselection	3232	3079	989.8	35.92	2012	40.55	31.9	72.4
'$\gamma\gamma$' + q$\bar{\mathrm{q}}(\gamma)$	5	5.53	1.84	0.02	0.18	3.49	21.4	45.3
4-fermion	1	0.36	0.05	0.00	0.18	0.13	18.9	34.9

Table 1: The remaining numbers of events in category (A) after each cut for various background processes normalised to 10.0 pb^{-1} and for data. For two typical signals, the fraction of events identified in category (A) after each cut relative to the total number of events for all categories combined is given. The chargino signal corresponds to $m_{\tilde{\chi}_1^+} = 75$ GeV and $m_{\tilde{\chi}_1^0} = 55$ GeV. The neutralino signal corresponds to $m_{\tilde{\chi}_2^0} = 100$ GeV and $m_{\tilde{\chi}_1^0} = 50$ GeV.

3.2   Category B: Hadronic decays with isolated leptons

In $\tilde{\chi}_1^+\tilde{\chi}_1^-$ events in which one of the $\tilde{\chi}_1^{\pm}$ decays leptonically, the events tend to fall into category (B). The fraction of $\tilde{\chi}_1^+\tilde{\chi}_1^-$ events falling into category (B) is approximately 45% including the region where the difference between $m_{\tilde{\chi}_1^{\pm}}$ and $m_{\tilde{\chi}_1^0}$ is 5 GeV or less. Since the virtual Z in the $\tilde{\chi}_2^0$ decay results in an event with either a pair of leptons or a multihadronic final state, the fraction of $\tilde{\chi}_2^0\tilde{\chi}_1^0$ events in this category is negligible. The counts of preselected events for the backgrounds and two typical chargino signals are shown in Table 2.

The most significant backgrounds for this category are W$^+$W$^-$ events and two-photon events. The P_t distribution, which was used to reject the two-photon background, is shown

in Fig. 1(c) for the events in category (B) after the preselection. Background events from two-photon processes are concentrated in the low P_t region.

As in category (A) several cuts were applied to ensure the events were well measured. The visible energy in the region of $|\cos\theta| > 0.9$ was required to be less than 20% of the total visible energy. The polar angle of the missing momentum direction θ_{miss} was required to satisfy $|\cos\theta_{\mathrm{miss}}| < 0.95$. These cuts rejected many of the $e^+e^- \to Z\gamma$ and two-photon events.

To reduce two-photon events further, the event P_t was required to be greater than 5 GeV. The two-photon background was also reduced by dividing the event, including the lepton, into two jets using the Durham jet algorithm and then requiring that the acoplanarity angle between the two reconstructed jets be greater than $20°$. To reduce background from two-photon processes, a harder cut on the acoplanarity angle was applied if at least one of the polar angles of the jet, θ_{jet}, satisfied $|\cos\theta_{\mathrm{jet}}| > 0.65$ and if P_t was smaller than 8 GeV. In this case, the acoplanarity angle was required to be between $(240° - 30° \times P_t)$ and $160°$, where P_t is in GeV. The counts of events remaining after the category (B) two-photon cuts are shown in the third row of Table 2.

To reduce the $W^+W^- \to q\bar{q}\ell\nu$ background, events with a high energy jet and a mass consistent with a W when the lepton was removed were rejected. An event was rejected if its highest lepton energy, E_ℓ^{max}, exceeded 30 GeV. The invariant mass of the event excluding the highest energy lepton, M_{rest}, was required to be smaller than $(N_{\mathrm{jet}}/3) \times 40$ GeV, where N_{jet} is the number of reconstructed jets. Chargino-pair and W-pair events that fall into category (B) naturally have three jets (including one isolated lepton jet). The N_{jet} dependent cut was needed since M_{rest} increases with increasing N_{jet} for both signal and W-pair background. The M_{rest} distribution is shown in Fig. 1(d) for data, the simulated background and a typical signal sample. The W boson peak can be seen in the background simulation. The visible energy of the event, E_{vis}, was required to be smaller than $(0.2 \times N_{\mathrm{jet}}/3 + 0.3) \times \sqrt{s}$. The dependence on N_{jet} was needed for the same reason as for the M_{rest} requirement. The counts of events remaining after the category (B) four-fermion cuts are shown in the fourth row of Table 2. For events falling into category (B) the detection efficiency for $\tilde{\chi}_1^+\tilde{\chi}_1^-$ events is 40–65% for ΔM_+ between 10 GeV and $m_{\tilde{\chi}_1^+}$–20 GeV. For larger ΔM_+ the efficiency drops to 30–35% due to the cuts against the W bosons. At $\Delta M_+ = 5$ GeV, the efficiency is 15–20%. No events passing the category (B) requirements were observed. The number of background events expected in this category is 0.14 events.

3.3   Category C: Low multiplicity decays

Purely leptonic events or hadronic events with small ΔM_+ or ΔM_0 tend to fall into category (C). The fraction of $\tilde{\chi}_1^+\tilde{\chi}_1^-$ events falling into category (C) is about 10% for most of the $(m_{\tilde{\chi}^\pm}, m_{\tilde{\chi}_1^0})$ region. However, if ΔM_+ is 5 GeV or less, the fraction increases to 40%. For $\tilde{\chi}_1^0\tilde{\chi}_{2,3}^0$ events the fraction is typically 13% but increases to approximately 80% when the mass difference between $\tilde{\chi}_{2,3}^0$ and $\tilde{\chi}_1^0$ is 5 GeV or less.

Events were split into two jets using the Durham jet algorithm and cuts were applied either to the jets or to the whole event. The component of P_t perpendicular to the event thrust axis, a_t, normalized to the beam energy (E_{beam}) is shown in Fig. 1(e) for category (C) events after the preselection cuts. As described below, this quantity is used to reduce the background from back-to-back lepton pairs, which tend to have small a_t even when P_t is large. The counts of

cut	data	net bkg.	$q\bar{q}(\gamma)$	$\ell^+\ell^-(\gamma)$	'$\gamma\gamma$'	4-f	$\tilde{\chi}_1^+\tilde{\chi}_1^-$ (%)	$\tilde{\chi}_1^+\tilde{\chi}_1^-$ (%)
Category (B)	–	–	–	–	–	–	67.3	45.1
Preselection	4288	3909	18.0	27.7	3850	13.2	66.5	43.7
'$\gamma\gamma$'	5	3.16	0.08	0.16	0.04	2.89	37.0	30.9
4-fermion	0	0.14	0.00	0.02	0.04	0.09	37.0	30.0

Table 2: The remaining numbers of events in category (B) after each cut for various background processes normalised to 10.0 pb^{-1} and for data. For two typical signals, the fraction of events identified in category (B) after each cut relative to the total number of events for all categories combined is given. The first chargino signal corresponds to $m_{\tilde{\chi}_1^+} = 80$ GeV and $m_{\tilde{\chi}_1^0} = 70$ GeV. The second chargino signal corresponds to $m_{\tilde{\chi}_1^+} = 80$ GeV and $m_{\tilde{\chi}_1^0} = 40$ GeV. The disagreement between the data and net background preselection counts is due to incomplete modelling of the two-photon background at low P_t.

preselected events for the backgrounds and a typical chargino and neutralino signal are shown in Table 3. The disagreement between the count of preselected data and background events is attributed to incomplete modelling of the two-photon background at low P_t.

Two-photon events represent the most serious background in category (C). Two-photon events were removed by requiring that the events have a significant P_t. For events with acoplanarity angle between the two jets greater than 50° and the missing momentum direction well within the acceptance, the P_t was required to be greater than 4 GeV. For events with acoplanarity angle less than 50°, a cut on low a_t rejected back-to-back lepton pairs with significant P_t (mainly tau pairs) thus allowing a looser P_t cut to be applied. Thus, for events with acoplanarity less than 50°, a_t greater than 2 GeV and with a_t being significant with respect to the longitudinal momentum (P_z) of the event (i.e. $|P_z|/\sqrt{a_t^2 + P_z^2} < 0.95$), the P_t was required to be greater than 2.8 GeV. The $e^+e^-\mu^+\mu^-$ background was reduced by rejecting events with a track segment in the muon chambers, hadron calorimeter strips or central detector in the very forward region within ±1 rad in ϕ around the missing transverse momentum direction. This eliminated background events with an escaping muon in the forward direction. The visible mass was required to be greater than 3 GeV to eliminate $e^+e^-\tau^+\tau^-$ events in which one of the taus decayed into a very low momentum lepton. Further reduction of the two-photon background with escaping particles was obtained by requiring the event to be electrically neutral. In addition, the low multiplicity environment allowed a harder cut to be applied on the SW energy than was used in the preselection cuts. To reduce the residual two-photon background, events were rejected if one of the jets had $|\cos\theta| > 0.75$. The counts of events remaining after the category (C) two-photon cuts are show on the third row of Table 3.

The $\ell^+\ell^-(\gamma)$ background was removed by requiring that the acoplanarity angle between the jets be greater than 30°. The event counts remaining after this $\ell^+\ell^-(\gamma)$ cut are shown in the fourth row of Table 3.

To reduce the W^+W^- background, events were rejected if one of the jets had an energy greater than 12 GeV. The event counts remaining after this four-fermion cut are shown in the fifth row of Table 3.

The distributions of the visible mass for background and simulated signals after all cuts excluding the visible mass cut are shown in Fig. 1(f). For events falling into category (C) the detection efficiency for $\tilde{\chi}_1^+\tilde{\chi}_1^-$ events with ΔM_+ between 5 GeV and 10 GeV is 11–24% and

for $\tilde{\chi}_2^0\tilde{\chi}_1^0$ events with ΔM_0 between 5 GeV and 10 GeV it is 5–22%. The detection efficiency for $\tilde{\chi}_1^+\tilde{\chi}_1^-$ ($\tilde{\chi}_2^0\tilde{\chi}_1^0$) events becomes negligible if ΔM_+ (ΔM_0) is greater than 20 GeV due to the jet energy cut. The total number of background events expected in category (C) is 0.20. One candidate event was observed in category (C). It has two reconstructed charged tracks, a P_t of 6.0 GeV, an acoplanarity angle of 149° and its visible energy is 9.4 GeV. It is consistent with being an $e^+e^-\tau^+\tau^-$ background event.

cut	data	net bkg.	$q\bar{q}(\gamma)$	$\ell^+\ell^-(\gamma)$	'$\gamma\gamma$'	4-f	$\tilde{\chi}_1^+\tilde{\chi}_1^-$ (%)	$\tilde{\chi}_2^0\tilde{\chi}_1^0$ (%)
Category (C)	–	–	–	–	–	–	37.6	49.8
Preselection	17034	13410	0.71	2809	10580	19.94	31.8	43.5
'$\gamma\gamma$'	10	6.20	0.00	3.93	0.15	2.12	4.2	10.6
$\ell^+\ell^-(\gamma)$	5	2.53	0.00	0.70	0.15	1.69	4.2	10.6
4-fermion	1	0.20	0.00	0.01	0.15	0.04	4.0	10.6

Table 3: The remaining numbers of events in category (C) after each cut for various background processes normalised to 10.0 pb^{-1} and for data. For two typical signals, the fraction of events identified in category (C) after each cut relative to the total number of events for all categories combined is given. The chargino signal corresponds to $m_{\tilde{\chi}_1^+} = 65$ GeV and $m_{\tilde{\chi}_1^0} = 60$ GeV. The neutralino signal corresponds to $m_{\tilde{\chi}_2^0} = 85$ GeV and $m_{\tilde{\chi}_1^0} = 75$ GeV. The disagreement between the data and net background preselection counts is due to incomplete modelling of the two-photon background at low P_t.

4 Results

The total background expected for this search is the sum of the background contributions from each category. The total background expected for 10.0 pb^{-1} is 0.70 events. The net efficiency for each mass pair combination was obtained by taking the sum of the efficiencies for each category weighted by the fraction of signal events falling into the category. Typical overall efficiencies for $\tilde{\chi}_1^+\tilde{\chi}_1^-$ and $\tilde{\chi}_1^0\tilde{\chi}_2^0$ events are given in Table 4.

$m_{\tilde{\chi}_1^\pm} = 80$ GeV, $m_{\tilde{\chi}_1^0}$ (GeV)=	75	70	60	40	10
detection efficiency (%)	12	48	56	48	20
$m_{\tilde{\chi}_2^0} = 100$ GeV, $m_{\tilde{\chi}_1^0}$ (GeV)=	60	50	40	30	20
detection efficiency (%)	32	34	28	20	14

Table 4: The first two rows show the detection efficiencies for some typical points in percent for the three categories combined for $\tilde{\chi}_1^+\tilde{\chi}_1^-$ followed by the decay $\tilde{\chi}_1^\pm \to \tilde{\chi}_1^0 W^{*\pm}$. The dependence on $m_{\tilde{\chi}_1^+}$ is small. The last two rows show the detection efficiencies for some typical points in percent for the three categories combined for $\tilde{\chi}_1^0\tilde{\chi}_2^0$ followed by the decay $\tilde{\chi}_2^0 \to \tilde{\chi}_1^0 Z^*$.

4.1 Systematic Errors

The systematic error in the number of expected signal events was due to the following sources: the measurement of the integrated luminosity (0.6%), Monte Carlo statistics in the various signal samples and the interpolation errors of the efficiencies at an arbitrary point of $m_{\tilde{\chi}_1^+}$ ($m_{\tilde{\chi}_2^0}$) and $m_{\tilde{\chi}_1^0}$ (2–10%), modelling of the cut variables in the Monte Carlo simulations (2–4%), errors due to fragmentation uncertainties in hadronic decays ($< 2\%$) and effects of detector calibration ($< 1\%$). These systematic errors were considered to be independent and were added in quadrature.

The systematic errors in the expected number of background events used to obtain the limits were due to Monte Carlo statistics in the simulated background events, uncertainties in the amount of two-photon background estimated by fitting the P_t distributions of simulated two-photon events and the data (30%) and uncertainties in the simulation of the four-fermion processes which were estimated by comparing the EXCALIBUR and the grc4f [24] generators (11%). A 100% systematic error was assumed for the number of background events expected for the $q\bar{q}(\gamma)$ and $\ell^+\ell^-(\gamma)$ states. Therefore, the total expected number of background events is estimated to be 0.70 ± 0.19 (0.05 ± 0.05 from $q\bar{q}(\gamma)$, 0.02 ± 0.02 from $\ell^+\ell^-(\gamma)$, 0.36 ± 0.18 from two photon processes and 0.26 ± 0.03 from four-fermion final states).

4.2 Limits

The 95% confidence level (C.L.) upper limits on the production cross-sections for $\tilde{\chi}_1^+\tilde{\chi}_1^-$ and $\tilde{\chi}_1^0\tilde{\chi}_2^0$ were first obtained assuming specific decay modes of $\tilde{\chi}_1^\pm \rightarrow \tilde{\chi}_1^0 W^{*\pm}$ and $\tilde{\chi}_2^0 \rightarrow \tilde{\chi}_1^0 Z^*$. From the observation of two events in a Poisson process with a predicted background of 0.70 ± 0.19 events, and the signal detection efficiencies and their uncertainties, exclusion regions were determined using the procedure outlined in [25]. As suggested in [25] a numerical convolution was used to include the background uncertainty. These limits do not depend on the details of the SUSY models, but some production angular distributions had to be assumed to estimate detection efficiencies. It was checked that the limits excluding a given combination of gaugino masses are valid for all sets of MSSM parameters resulting in the mass combination.

Contours of the upper limits for the $\tilde{\chi}_1^+\tilde{\chi}_1^-$ cross-sections are shown in Fig. 3(a) assuming $\tilde{\chi}_1^+ \rightarrow \tilde{\chi}_1^0 W^*$ with 100% branching fraction. Similarly, the contours of the upper limit for the $\tilde{\chi}_2^0\tilde{\chi}_1^0$ cross-sections are shown assuming 100% branching fraction for $\tilde{\chi}_2^0 \rightarrow \tilde{\chi}_1^0 Z^*$ (Fig. 3(b)). The Standard Model branching fractions were used for the W^{*+} and Z^* decays, including the invisible decay mode $Z^* \rightarrow \nu\bar{\nu}$ and taking account of phase-space effects for decays into heavy particles. The previous limits obtained at 130 and 136 GeV [2] are combined with the limits at 161 GeV as shown in the figures, assuming that the cross-sections are proportional to $\tilde{\beta}/s$, where $\tilde{\beta}$ is the momentum of the final state $\tilde{\chi}_1^+$ or $\tilde{\chi}_2^0$ in the centre-of-mass system.

If the cross-section for $\tilde{\chi}_1^+\tilde{\chi}_1^-$ is larger than 3.5 pb and ΔM_+ is larger than 6 GeV, we can exclude the $\tilde{\chi}_1^+$ mass up to the kinematical limit at the 95% C.L. for $\tilde{\chi}_1^+$ decay via W^*. We can also exclude the $\tilde{\chi}_2^0$ mass up to the kinematical boundary of $(m_{\tilde{\chi}_2^0} + m_{\tilde{\chi}_1^0}) < \sqrt{s}$ at the 95% C.L. for $8 \leq \Delta M_0 \leq 90$ GeV, if the cross-section for $\tilde{\chi}_1^0\tilde{\chi}_2^0$ is larger than 8 pb.

The results of the above searches can be interpreted within the framework of the MSSM where the gaugino sector of the theory is dominantly determined by three parameters: the SU(2) gaugino mass parameter (M_2), mixing parameter of the two Higgs field doublets (μ) and

the ratio of the vacuum expectation values associated with the two neutral scalar Higgs fields ($\tan\beta$). The sfermion spectrum is further constrained by assuming soft symmetry breaking at the Grand Unification (GUT) scale with a common mass scale m_0 (defined at the GUT scale) [26]. A light m_0 results in low values of the masses of the $\tilde{\nu}$ and $\tilde{\ell}$, thereby enhancing t-channel exchange diagrams that may have destructive interference with s-channel diagrams, reducing the cross-section for chargino production. Small values of m_0 also tend to enhance the leptonic branching ratio of charginos. On the other hand, fixing m_0 to high values decouples the $\tilde{\nu}$ from the theory, thereby enhancing the chargino production rate. We present results for two cases: $m_0 = 1$ TeV and the smallest m_0 consistent with light $\tilde{\ell}$ and $\tilde{\nu}$ not yet excluded, namely $m_{\tilde{\ell}} > 45.0$ GeV, $m_{\tilde{\nu}} > 41.8$ GeV, and $m_{\mathrm{h}^0} > 45$ GeV [27].

Production cross-sections and branching fractions are calculated according to the MSSM model, and the total number of $\tilde{\chi}_1^+\tilde{\chi}_1^-$, $\tilde{\chi}_1^0\tilde{\chi}_2^0$ and $\tilde{\chi}_1^0\tilde{\chi}_3^0$ events expected to be observed was found using the determined efficiencies. The efficiency for detecting $\tilde{\chi}_1^0\tilde{\chi}_3^0$ events, even for decays through SUSY Higgs bosons, was found to be greater than for $\tilde{\chi}_1^0\tilde{\chi}_2^0$ events, but we conservatively use the efficiency functions for $\tilde{\chi}_1^0\tilde{\chi}_2^0$. The decay involving $\tilde{\chi}_{2,3}^0 \rightarrow \tilde{\ell}\ell$ when $m_{\tilde{\chi}_{2,3}^0} > m_{\tilde{\ell}}$ and the decay $\tilde{\chi}_{2,3}^0 \rightarrow \tilde{\chi}_1^0\gamma$ are assumed to be undetectable in this analysis.

Figures 4(a) for $\tan\beta = 1.5$ and 4(b) for $\tan\beta = 35$ show the resulting exclusion regions in the M_2-μ plane. The region of M_2-μ excluded is close to the kinematical boundary for chargino production if m_0 is 1 TeV, and is improved significantly with respect to the LEP1.5 result [2] for the light-m_0 scenario. In the $m_{\tilde{\chi}_1^0}$-$m_{\tilde{\chi}_1^\pm}$ plane, Fig. 5 shows the corresponding 95% C.L. exclusion regions for $\tan\beta$=1.5 in (a) and $\tan\beta$=35 in (b) for the following scanned regions of the MSSM parameters: $0 \leq M_2 \leq 1500$ GeV, $|\mu| \leq 500$ GeV, A (the trilinear coupling) $= \pm M_2$, $\pm m_0$ and 0, and $m_{\mathrm{A}^0} = 25$, 100 and 500 GeV. The typical scan step was 0.1 GeV. The scanned ranges of parameters were checked to be large enough so that the exclusion regions presented change negligibly for larger or different ranges. The analogous exclusion region in the $m_{\tilde{\chi}_1^0}$-$m_{\tilde{\chi}_2^0}$ plane is shown in Fig. 5(c) and (d). Not as much of the accessible region of mass space for neutralino production is excluded because of the smaller predicted cross-sections for neutralinos. The portion of the excluded region extending beyond the kinematic limit $m_{\tilde{\chi}_1^0} + m_{\tilde{\chi}_2^0} < 161$ GeV is due to the exclusion of chargino production for relevant MSSM parameters. The difference in the detection efficiencies due to variations in the angular distributions resulting from using different MSSM parameters corresponding to the same mass combination was included in the uncertainty on the efficiencies when calculating the 95% C.L. limits. The lower limits of the chargino and neutralino masses are listed in Table 5. The limits on the $\tilde{\chi}_3^0$ mass are obtained mainly from excluded regions in the MSSM parameter space resulting from the direct search for lighter neutralinos and $\tilde{\chi}_1^\pm$.

5 Summary and Conclusion

A data sample corresponding to an integrated luminosity of 10.0 pb^{-1} at $\sqrt{s} =$161 GeV collected with the OPAL detector has been analysed to search for pair production of charginos and neutralinos predicted by supersymmetric theories. Two events survived the cuts. The expected number of background events is 0.70 ± 0.19. Using these results the exclusion limits on $\tilde{\chi}_1^\pm$ and $\tilde{\chi}_{2,3}^0$ production are significantly improved with respect to the results obtained at $\sqrt{s} =$130 GeV and 136 GeV.

Mass	$\tan\beta = 1.5$		$\tan\beta = 35$	
	Min. m_0	$m_0 = 1$ TeV	Min. m_0	$m_0 = 1$ TeV
$m_{\tilde{\chi}_1^\pm}$ (GeV)	> 62.0	> 78.5	> 66.5	> 78.8
$m_{\tilde{\chi}_1^0}$ (GeV)	> 12.0	> 30.3	> 35.8	> 41.3
$m_{\tilde{\chi}_2^0}$ (GeV)	> 45.3	> 51.9	> 67.2	> 80.0
$m_{\tilde{\chi}_3^0}$ (GeV)	> 86.3	> 94.3	> 112.5	> 112.5

Table 5: The lower limits at 95% C.L. obtained on the chargino mass $m_{\tilde{\chi}_1^+}$, and the masses of the three lightest neutralinos. These limits are given for $\Delta \tilde{M}_+ \geq 10$ GeV and $\Delta M_0 \geq 10$ GeV and two cases are considered: $m_0 = 1$ TeV and the smallest m_0 possible that complies with the LEP1 $\tilde{\ell}$, $\tilde{\nu}$ and h^0 limits.

6   Acknowledgements

References

[1] Y. Gol'fand and E. Likhtam, JETP Lett. 13 (1971) 323;
D. Volkov and V. Akulov, Phys. Lett. B46 (1973) 109;
J. Wess and B. Zumino, Nucl. Phys. B70 (1974) 39.

[2] OPAL Collab., G. Alexander *et al.*, Phys. Lett. B377 (1996) 181.

[3] ALEPH Collab., D. Buskulic *et al.*, Phys. Lett. B373 (1996) 246;
DELPHI Collab., P. Abreu *et al.*, 'Search for the lightest chargino at $\sqrt{s} = 130$ and 136 GeV in DELPHI', CERN preprint PPE/96-75 (1996);
L3 Collab., M. Acciarri *et al.*, Phys. Lett. B377 (1996) 289.

[4] CDF Collab., F. Abe *et al.*, Phys. Rev. Lett. 76 (1996) 4307;
D0 Collab., S. Abachi *et al.*, Phys. Rev. Lett. 76 (1996) 2228.

[5] H. P. Nilles, Phys. Rep. 110 (1984) 1;
H. E. Haber and G. L. Kane, Phys. Rep. 117 (1985) 75.

[6] A. Bartl, H. Fraas and W. Majerotto, Z. Phys. C30 (1986) 441;
A. Bartl, H. Fraas and W. Majerotto, Z. Phys. C41 (1988) 475;
A. Bartl, H. Fraas, W. Majerotto and B. Mösslacher, Z. Phys. C55 (1992) 257.

[7] M. Chen, C. Dionisi, M. Martinez and X. Tata, Phys. Rep. 159 (1988) 201;
J. L. Feng and M. J. Strassler, Phys. Rev. D51 (1995) 4661.

[8] OPAL Collab., K. Ahmet *et al.*, Nucl. Instr. Meth. A305 (1991) 275;
P.P. Allport *et al.*, Nucl. Instr. Meth. A346 (1994) 476;
B.E. Anderson *et al.*, IEEE Trans. on Nucl. Science 41 (1994) 845.

[9] E. Accomando *et al.*, 'Event Generators for Discovery Physics', hep-ph/9602203, Feb. 1996.

[10] T. Sjöstrand, Comp. Phys. Comm. 39 (1986) 347;
T. Sjöstrand, PYTHIA 5.7 and JETSET 7.4 Manual, CERN-TH 7112/93.

[11] E. Boudinov *et al.*, '$\gamma\gamma$ Event Generators', hep-ph/9512371, Dec. 1995.

[12] G. Marchesini *et al.*, Comp. Phys. Comm. 67 (1992) 465.

[13] J.A.M. Vermaseren, Nucl. Phys. B229 (1983) 347.

[14] F.A. Berends, R. Pittau, R. Kleiss, Comp. Phys. Comm. 85 (1995) 437.

[15] S. Jadach, B. F. L. Ward, Z. Wąs, Comp. Phys. Comm. 79 (1994) 503.

[16] S. Jadach, W. Płaczek, B.F.L. Ward, in 'Physics at LEP2', eds. G. Altarelli, T. Sjöstrand and F. Zwirner, CERN 96-01, vol. 2 (1996).

[17] J. Allison *et al.*, Nucl. Instr. Meth. A317 (1992) 47.

[18] N. Brown and W.J. Stirling, Phys. Lett. B252 (1990) 657;
S. Bethke, Z. Kunszt, D. Soper and W.J. Stirling, Nucl. Phys. B370 (1992) 310;
S. Catani, Phys. Lett. B269 (1991) 432;
N. Brown and W.J. Stirling, Z. Phys. C53 (1992) 629.

[19] OPAL Collab., R. Akers *et al.*, Phys. Lett. B327 (1994) 411.

[20] OPAL Collab., R. Akers *et al.*, Z. Phys. C65 (1994) 17.

[21] OPAL Collab., P. Acton *et al.*, Z. Phys. C58 (1993) 523.

[22] OPAL Collab., R. Akers *et al.*, Z. Phys. C60 (1993) 199.

[23] OPAL Collab., G. Alexander *et al.*, Z. Phys. C52 (1991) 175.

[24] J. Fujimoto *et al.*, KEK-CP-046 (1996).

[25] R.D. Cousins and V.L. Highland, Nucl. Instr. Meth. A320 (1992) 331.

[26] M. Drees and M. M. Nojiri, Nucl. Phys. B369 (1992) 54;
M. Carena, S. Dimopolous, S. Raby and C.M.E. Wagner, Phys. Rev. D52 (1995) 4133.

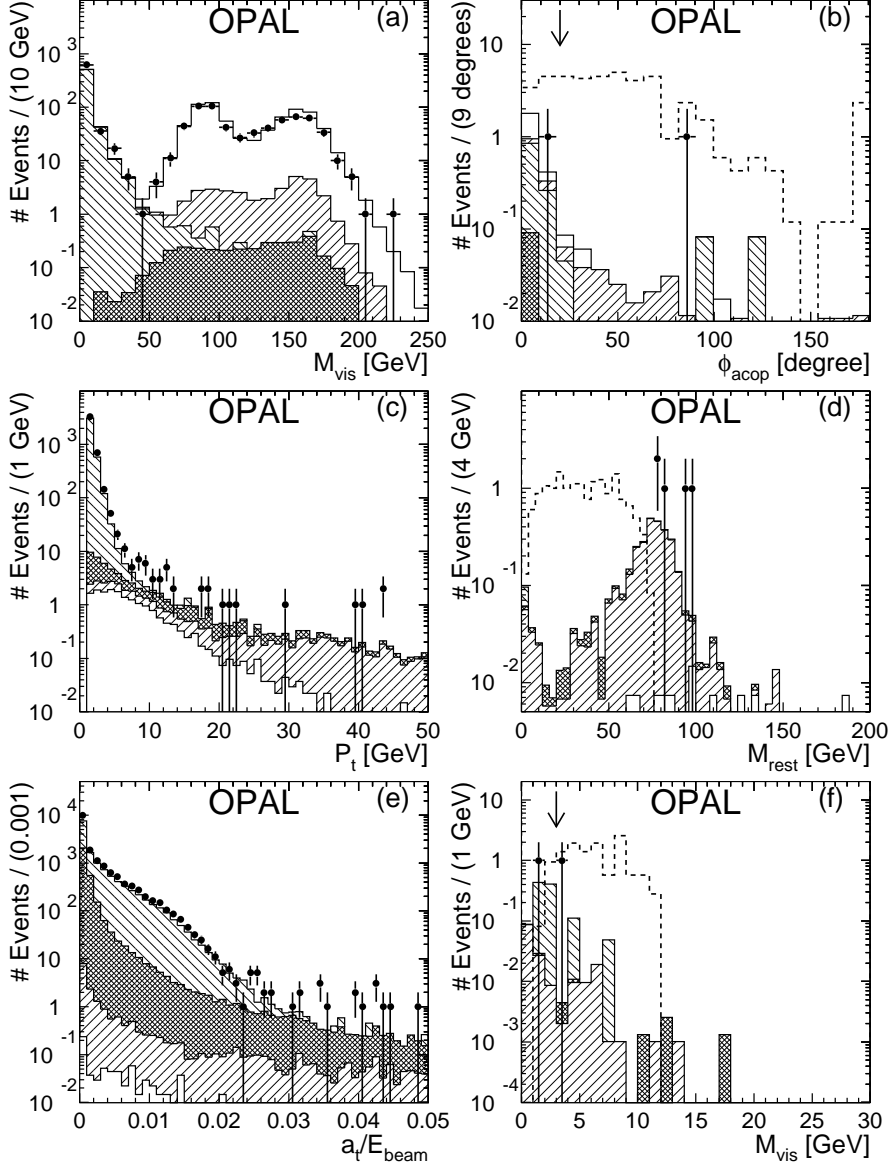[27] Particle Data Group, Phys. Rev. D50 (1994) 1173.

Figure 1: Distributions of some essential observables used to select chargino and neutralino events. The data are shown with error bars, and the predictions from the background processes are shown as histograms: dilepton events (double hatched area), two-photon processes (area with negative slope hatching), four-fermion processes including W-pair events (positive slope hatching area), and multihadronic events (open area). The distributions are as described in the text. In figure (b) the dashed line shows the prediction for a chargino signal with $m_{\tilde{\chi}_1^+} = 75$ GeV and $m_{\tilde{\chi}_1^0} = 55$ GeV. In figure (d) the dashed line shows the prediction for a chargino signal with $m_{\tilde{\chi}_1^+} = 80$ GeV and $m_{\tilde{\chi}_1^0} = 40$ GeV. In figure (f) the dashed line shows the prediction for a chargino signal with $m_{\tilde{\chi}_1^+} = 65$ GeV and $m_{\tilde{\chi}_1^0} = 60$ GeV. Where appropriate the arrows show where the analysis cuts were applied. The normalizations of the signal histograms are arbitrary.

17

Side view - plane of Thrust axis

Phi=183

Phi= 93.
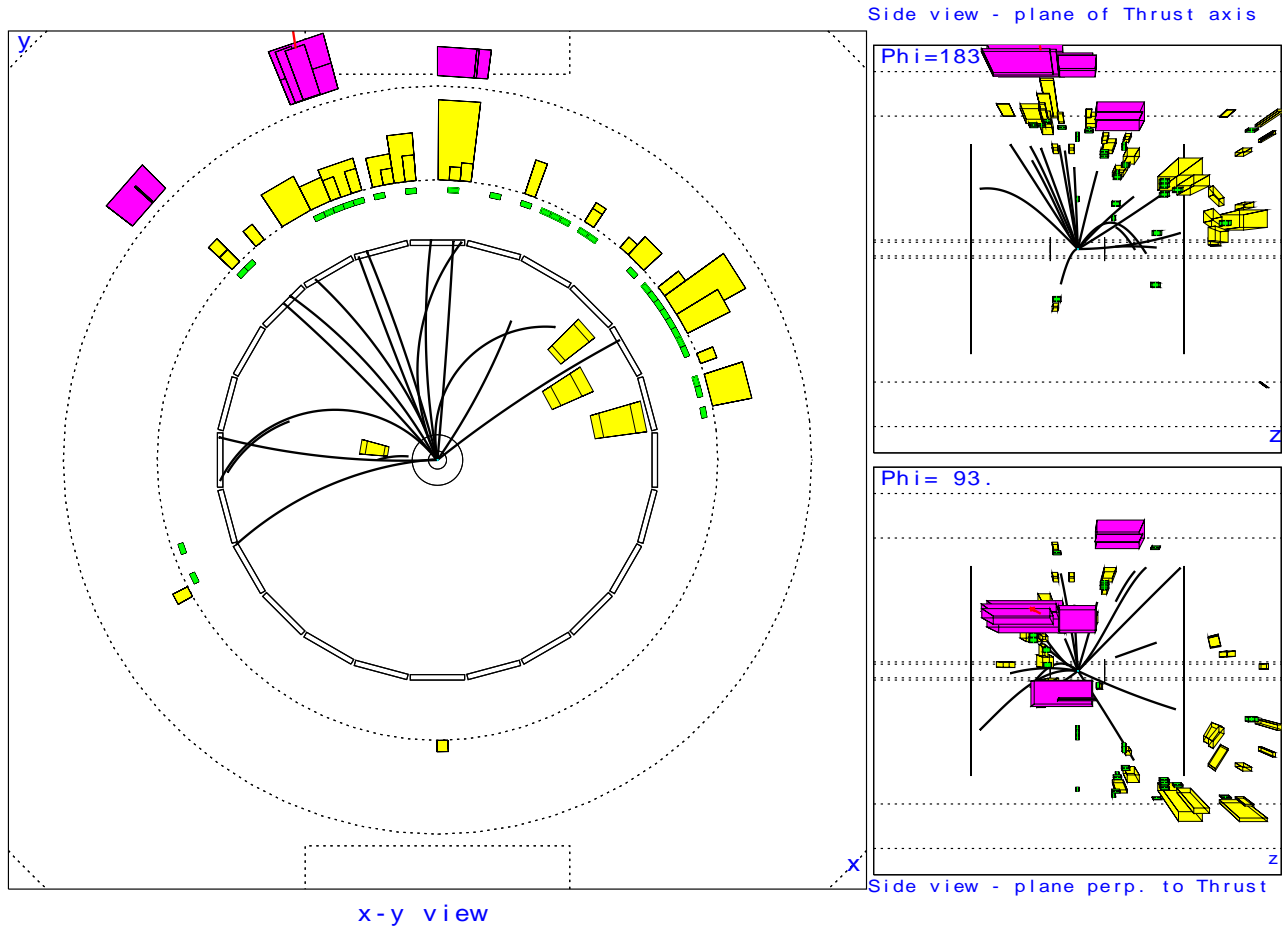
Side view - plane perp. to Thrust

x-y view

Figure 2: The event remaining in the data after application of all selection criteria in category (A). The dark lines represent fitted charged tracks in the tracking chambers. The light grey boxes indicate the relative amount of energy deposited in EM calorimeter clusters. The dark grey boxes indicate the relative amount of energy deposited in hadron calorimeter clusters. The large picture shows a view of the event transverse to the beam pipe. The pictures on the right show sideviews of the event.
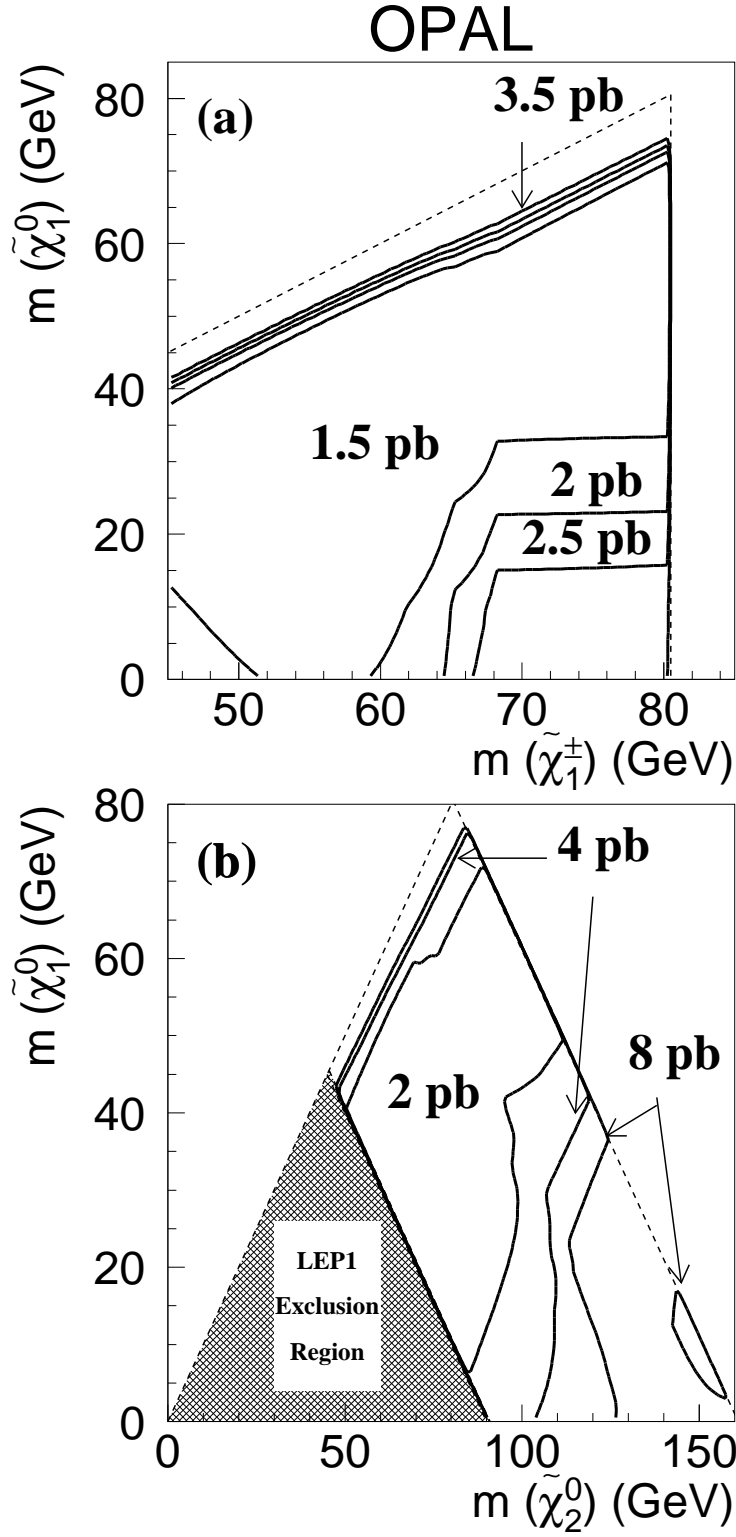
Figure 3: The contour plots of the 95% C.L. upper-limits on the production cross-sections at $\sqrt{s} = 161$ GeV for (a) $e^+e^- \rightarrow \tilde{\chi}_1^+ \tilde{\chi}_1^-$, and (b) $e^+e^- \rightarrow \tilde{\chi}_1^0 \tilde{\chi}_2^0$. The $\tilde{\chi}_1^+$ is assumed to decay into $\tilde{\chi}_1^0 W^{*+}$ with 100% branching fraction, and the $\tilde{\chi}_2^0$ is assumed to decay into $\tilde{\chi}_1^0 Z^*$ with 100% branching fraction. These limits have been obtained by combining the results of the present analysis and those at 130–136 GeV [2].
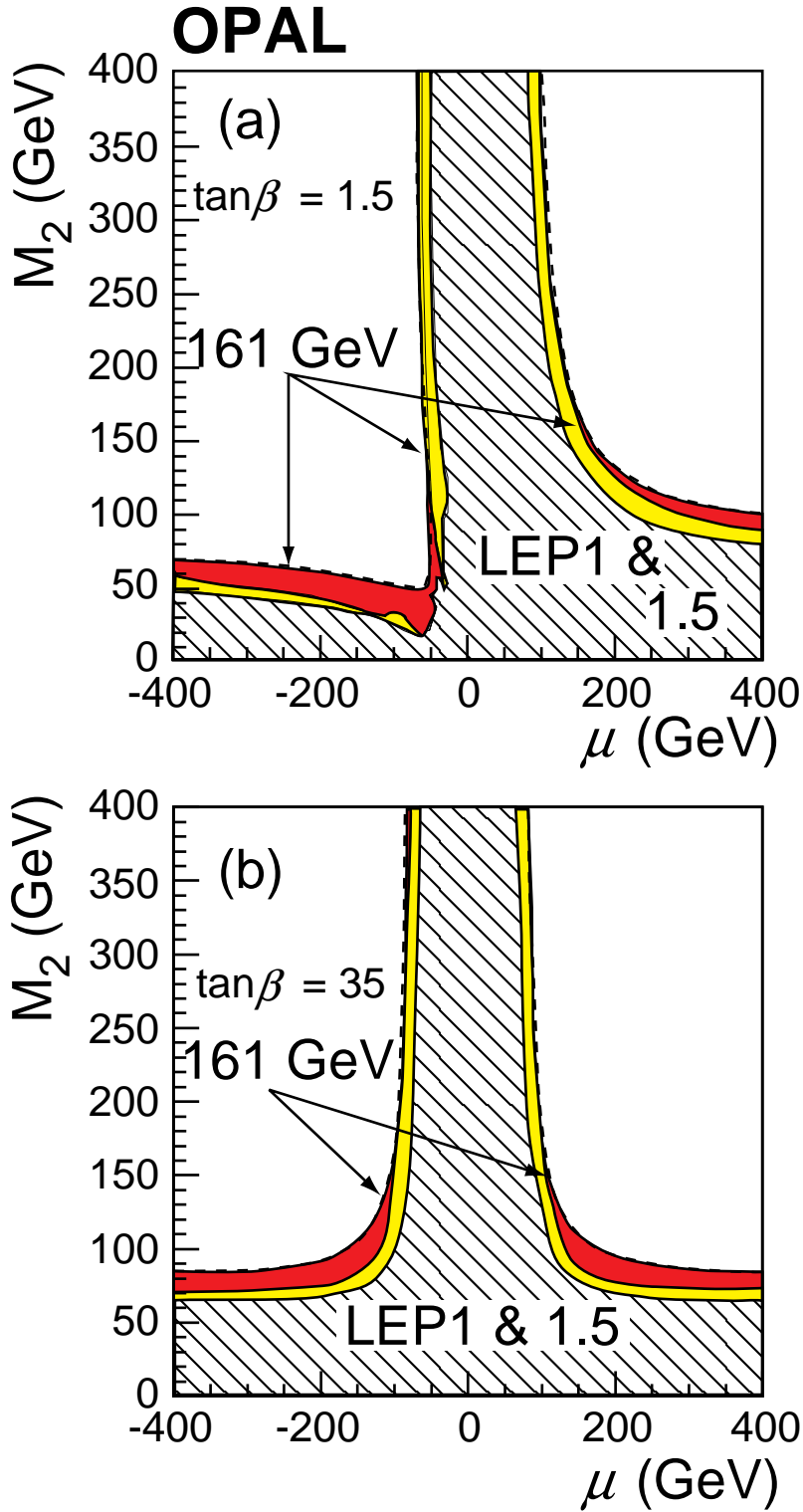
Figure 4: The exclusion contours in the M_2-μ plane for (a) $\tan\beta = 1.5$ and (b) $\tan\beta = 35$. The light shaded areas show the case of minimum m_0, and the dark shaded areas show the additional excluded region for $m_0 = 1$ TeV. The minimum m_0 is defined to be the smallest m_0 possible to comply with the limits on $\tilde{\ell}$, $\tilde{\nu}$ and h^0 at LEP1. The region excluded by the analysis of LEP1 and LEP1.5 data is also shown for the minimum m_0 case. The kinematical boundary at $\sqrt{s} = 161$ GeV for $\tilde{\chi}_1^+\tilde{\chi}_1^-$ production is shown by dashed lines.
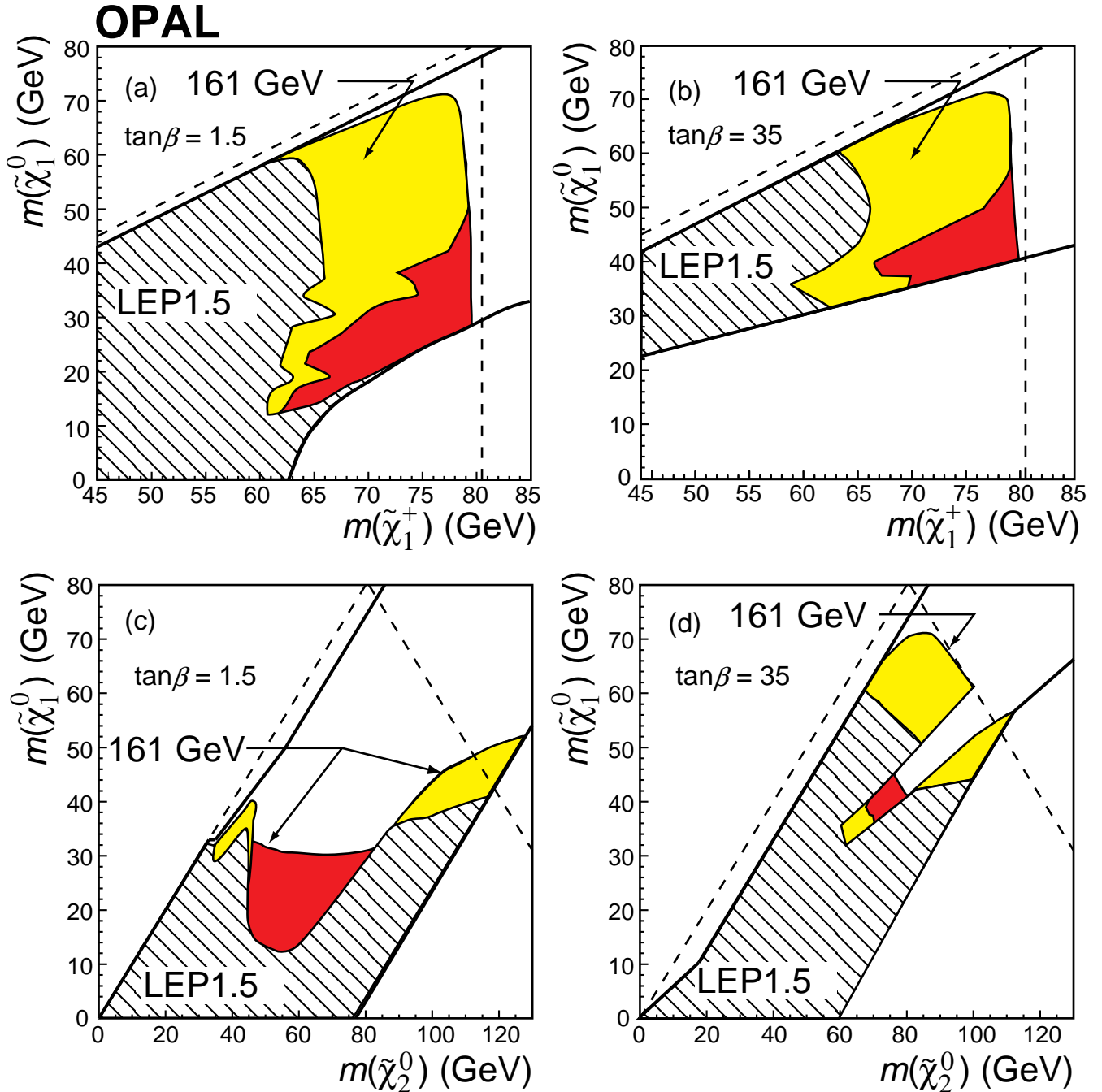
Figure 5: The 95% C.L. excluded region in the $m_{\tilde{\chi}_1^0}$-$m_{\tilde{\chi}_1^+}$ plane within the framework of the MSSM for the case of minimum m_0 (positive slope hatching area) and $m_0 = 1$ TeV (extending to dark shaded region) for (a) $\tan\beta = 1.5$ and (b) $\tan\beta = 35$. The region excluded by the analysis of LEP1 and LEP1.5 data is also shown for the minimum m_0 case (negative slope hatching area). The thick solid lines represent the theoretical bounds of the MSSM parameter space as given in the text. The kinematical boundaries for production and decay at $\sqrt{s} = 161$ GeV are shown by dashed lines. Similar plots for neutralino masses are shown in (c) for $\tan\beta = 1.5$ and (d) for $\tan\beta = 35$.